

Article

Genesis of the Beixiang Sb-Pb-Zn-Sn Deposit and Polymetallic Enrichment of the Danchi Sn-Polymetallic Ore Belt in Guangxi, SW China

Jing Wu ¹, Zhi Li ¹, Minjie Zhu ¹, Wenting Huang ², Juan Liao ^{1,3} , Jian Zhang ⁴ and Huaying Liang ^{2,*} ¹ School of Resources, Environment and Materials, Guangxi University, Nanning 530004, China² Key Laboratory of Mineralogy and Metallogeny, Guangzhou Institute of Geochemistry, Chinese Academy of Sciences, Guangzhou 510640, China³ University of Chinese Academy of Sciences, Beijing 100049, China⁴ Key Laboratory of Environment Change and Resources Use in Beibu Gulf, Ministry of Education, Nanning Normal University, Nanning 530001, China

* Correspondence: lianghy@gig.ac.cn

Abstract: Antimony deposits contain little Sn, whereas Sb and Pb are not the principally contained metal of granite-related Sn deposits. The Danchi Sn-metallogenic ore belt (DSOB) in southwestern China is characterized by Sn-Sb-Zn-Pb co-enrichment, yet the triggers are poorly constrained. The Beixiang deposit in the southern DSOB consists of stage I Sn-Zn and stage II Sb-Pb-Zn mineralization. Here, we analyzed the cassiterite U-Pb age, fluid inclusion H-O and sulfide Pb-S isotopes, and calcite trace elements of the Beixiang ores. By comparing with the Dachang and Mangchang Sn-polymetallic ore-fields within the DSOB, we constrained the timing of regional mineralization and revealed the processes causing the Sb-Pb co-enrichment. The cassiterite U-Pb dating yielded 90.6 ± 4.5 Ma (MSWD = 2.6), similar to the ages of the Dachang and Mangchang ore fields, indicating the Late Cretaceous mineralization event throughout the DSOB. The fluid inclusions from stage II ore have $\delta^{18}\text{O}_{\text{H}_2\text{O}}$ (−2.8 to −7.8‰) and $\delta\text{D}_{\text{V-SMOW}}$ (−90.5 to −59.3‰), and the synchronous calcite features have low REE contents, upward-convex REE patterns, and weak Eu anomalies. These suggest that the ore fluids were derived from meteoric water and oil field brine, which dissolved S and Pb from local strata as recorded by sulfide sulfur ($\delta^{34}\text{S}_{\text{V-CDT}} = -6.2$ to -4.0 ‰) and Pb isotopes. However, calcite from the stage I ore have higher REE contents and $(\text{La}/\text{Yb})_{\text{N}}$, with strong positive Eu anomalies, indicating that the Sn-rich ore fluids were released by greisenization of granite. Overall, we suggest that the combination of granitic magma- and oil field brine-derived fluids, rich in Sn-Zn and Sb-Pb-Zn, respectively, caused the co-enrichment of Sn-Sb-Pb-Zn in Beixiang and throughout the DSOB.



Citation: Wu, J.; Li, Z.; Zhu, M.; Huang, W.; Liao, J.; Zhang, J.; Liang, H. Genesis of the Beixiang Sb-Pb-Zn-Sn Deposit and Polymetallic Enrichment of the Danchi Sn-Polymetallic Ore Belt in Guangxi, SW China. *Minerals* **2022**, *12*, 1349. <https://doi.org/10.3390/min12111349>

Academic Editor: Maria Boni

Received: 26 September 2022

Accepted: 22 October 2022

Published: 25 October 2022

Publisher's Note: MDPI stays neutral with regard to jurisdictional claims in published maps and institutional affiliations.



Copyright: © 2022 by the authors. Licensee MDPI, Basel, Switzerland. This article is an open access article distributed under the terms and conditions of the Creative Commons Attribution (CC BY) license (<https://creativecommons.org/licenses/by/4.0/>).

Keywords: cassiterite U-Pb dating; ore-forming fluids; calcite REE; Beixiang polymetallic deposit; Danchi ore belt

1. Introduction

Granite-related W-Sn deposits are usually Pb-poor [1,2], e.g., the W-Sn deposits in the Nanling ore belt [3,4]. Sb is not enriched by fractionation in the granite [5]. Although some Sn deposits such as the well-known Potosi tin ore in the Andean Sn belt contain late Sb mineralization [6], Sb is not a metal that is principally contained in Sn deposits in the Sn belt [7]. Most Sb deposits were formed under low-temperature with no genetic link to the felsic magmatism [8,9], and Sb deposits with enrichment of Sn are rarely found. The Danchi Sn-polymetallic deposits are characterized by a high concentration of not only Sb but also Pb, a phenomenon that is yet to be well explained.

The Danchi Sn-polymetallic ore belt (length: over 100 km long) in South China (Figure 1a) contains several ore fields and a number of medium-small to giant-size Sn-polymetallic deposits. The ore belt is characterized by both enrichment of Sn-Zn and Sb-Pb,

which is uncommon in granite-related Sn deposits and has attracted much research attention [10–18]. Previous works found that the deposits in the Dachang and the Mangchang ore fields in the middle and northern ore belt (Figure 1a), respectively, have a genetic link to the late Yanshanian (~90 Ma) magmatism [11–14,19–25]. However, mineralization timing in the southern ore belt is still poorly constrained. It is still unclear if the Sn-polymetallic ores throughout the ore belt was caused by the same mineralization event.

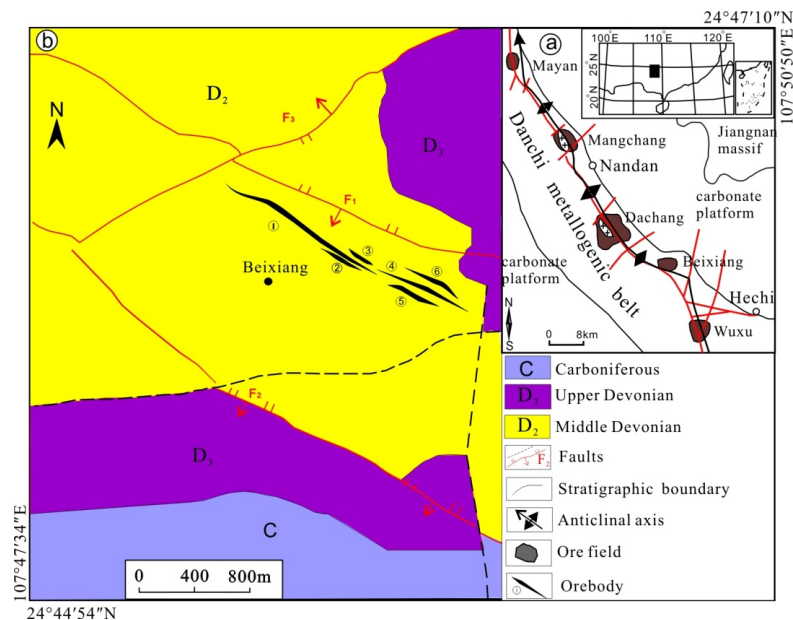


Figure 1. Sketch geological maps of the Danchi polymetallic belt (a) and the Beixiang deposit (b) [26].

The Beixiang polymetallic deposit in the southern part of the Danchi ore belt (Figure 1a) is especially Sb- and Pb-rich, whose age is still unconstrained. There are two stages of mineralization: stage I Zn-Sn mineralization has lower Sb-Pb enrichments, while stage II Sb-Pb-Zn mineralization has no Sn enrichment. The Beixiang deposit offers a good case for studying the processes causing the Sb-Pb co-enrichment, as well as the timing of the Sn polymetallic mineralization in the Danchi ore belt.

In this study, we conducted analyses on cassiterite U-Pb age, sulfide Pb-S isotopes, fluid inclusion H-O isotopes, and calcite REE geochemistry of the Beixiang deposit. The aims of this work are to reveal the formation processes of the Beixiang deposit and to shed light on the key Sb-Pb enrichment processes in the Danchi ore belt.

2. Ore Geology Setting

The Danchi Sn-polymetallic ore belt is located in southwest China (Figure 1a). The region underwent faulting and subsidence during the Devonian and Carboniferous periods, and folding in the Middle Triassic period [19]. During the Cretaceous period, many granitic intrusions emplaced in the Danchi belt under the extensional setting, which was associated with the subduction of Neo-Tethys [23]. There are many granite-related Sn-polymetallic ore fields throughout the belt. From the north to the south, they are the Mayang, Mangchang, Dachang, Beixiang and Wuxu ore fields (Figure 1). Previous cassiterite U-Pb and zircon U-Pb dating studies revealed that the Mangchang ore field in the north and the Dachang ore field in the middle part of the district were formed at 89.1–95.4 Ma and genetically related with the Cretaceous granitic magmatism in the region [11,12,14,25].

The Beixiang ore field is located in the Beixiang anticlinal axis in the southern Danchi ore belt. Outcropping sequences in the ore field include the Middle-Upper Devonian and Carboniferous ones. The Middle Devonian Donggangling Group outcrops in the middle of the Beixiang ore field, which consists of mudstone, marl, and limestone with chert interbeds, whereas the overlying Liujiang Group consists of chert and limestone (Figure 1).

The Upper Devonian Tongchejiang Group occurs in the southern and northeastern of the ore field, which consists of shale, mudstone, and limestone (Figure 1b). The Carboniferous strata outcrop in the southern part of the ore field, including mainly marl, limestone with banded chert, and quartz sandstone. On the other hand, Permian dolomitic limestone and chert and Triassic purple sandy conglomerate are distributed to the south and north of the ore field. The main faults in the Beixiang ore field are NW- or NE-trending. No intrusions outcrop in the ore field, but there is local marble formation in the ore field [26], indicating a high-temperature heat event, possibly derived from intrusions in the area. The gravity and magnetic anomaly also suggests that intrusions may be concealed at depth in the northern area of the Beixiang ore field [26,27].

The medium-size Beixiang Sb-Zn-Pb-Sn deposit occurs in the central Beixiang ore field and contains a reserve of 10,984 t Sb @ 1.26%, 43135 t Zn @ 3.62%, 27216 t Pb @ 3.12%, and 3560 t Sn @ 0.68%. The Beixiang orebodies are controlled by NW-trending faults hosted in the Middle Devonian Donggangling Group mudstone and marl. Bitumen locally occurs along the faults. Six orebodies (100–300 m long, 1.2–8.2 m thick) were delineated (Figure 1). The orebodies consist of a series of paralleled mineralized veins with thicknesses ranging from a few to tens of centimeters. Ore minerals in the veins are mainly sphalerite, jamesonite, pyrite, arsenopyrite, and galena with minor cassiterite, pyrrotite, and bismuthinite (Figure 2). Gangue minerals in the veins are mainly calcite, siderite, and sericite with minor quartz (Figure 2). These minerals show commonly euhedral to subhedral textures. It is common that jamesonite replaces or cut sphalerite (Figure 2d).

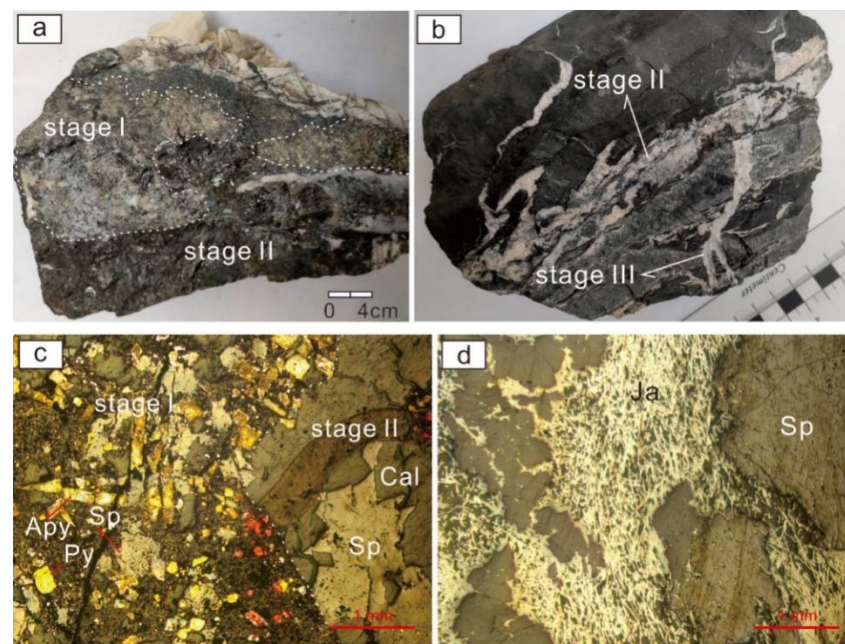


Figure 2. Photos showing the relationship among different stage mineralization. (a) Stage I mineralization is cut and enclosed by stage II mineralization. (b) Stage II mineralization is cut by stage III calcite-quartz vein. (c) Stage I mineralization consists of sphalerite, arsenopyrite and pyrite and stage II mineralization consists of sphalerite and calcite. (d) Jamesonite replaces or cut sphalerite in Stage II mineralization. Cal: calcite, Apy: arsenopyrite, Sp: sphalerite, Ja: jamesonite.

The ore vein textural relationships indicate that the Beixiang rock alteration/mineralization comprises three stages (Figures 2 and 3): stage I Zn-Sn mineralization, stage II Sb-Pb-Zn mineralization, and stage III calcite-quartz vein. Stage I mineralization occurs primarily at a relatively deep part of orebodies (below 65 m relative to sea levels) and is rarely observed. This stage mineralization occurs as irregular and small patches that are cut and enclosed by stage II mineralization (Figure 2a). Stage I mineralization

contains mainly sphalerite, cassiterite, arsenopyrite and pyrite, with minor pyrrhotite and bismuthinite. Gangue minerals in this stage include mainly calcite, with minor quartz and chlorite. Stage II mineralization is the main-ore stage, it widely occurs and represents the main mining target in the Beixiang deposit. Ores in stage II mainly show vein and massive structures (Figure 2a,b). Stage II mineralization contains sphalerite, jamesonite, galena, and pyrite. Gangue minerals in this stage mainly include calcite, siderite, and sericite, with minor quartz and bitumen. Stage III occurs locally and comprises calcite and quartz without ore minerals. Ore-related alteration is generally weak, including carbonization, silicification, and pyritization with minor chloritization. Furthermore, the Middle Devonian Donggangling Group limestone is locally recrystallized into marble [26].

| Mineral | stage I | stage II | stage III |
|--------------|------------|------------|------------|
| cassiterite | ██████████ | | |
| arsenopyrite | ██████████ | | |
| pyrite | ██████████ | ██████████ | ██████ |
| sphalerite | ██████████ | ██████████ | |
| jamesonite | | ██████████ | |
| galena | | ██████████ | |
| pyrrhotite | ██████████ | | |
| calcite | ██████████ | ██████████ | ██████████ |
| siderite | ██████████ | ■ | |
| quartz | ██████ | ██████ | ██████ |
| sericite | ██████ | ██████ | |
| chlorite | ██████ | | |
| bitumen | ██████ | ██████ | |

Figure 3. Paragenetic sequence of the different mineralization stages at Beixiang.

3. Samples and Analytical Methods

Ore samples were collected from various levels (10, 40, 65, 80, 130, and 140 m relative to sea level) within the Beixiang mine. Stage I ore samples are rather limited and only collected from 10 m and 40 m levels, whereas stage II ore samples could be collected from all levels. One cassiterite sample in stage I ore was used for in situ cassiterite U-Pb dating. Because it is hard to separate enough pure sulfide (sphalerite, arsenopyrite, and pyrite) and cassiterite in the rare stage I ore samples, isotopic (H, O, Pb, S) compositions of stage I could be not obtained. Sulfides (sphalerite, jamesonite, and pyrite) in stage II ore samples are relatively abundant and easily separated, and isotopic compositions in these ore minerals could directly represent the isotopic compositions of the ore-forming system; thus, isotopic (H, O, Pb, S) compositions of sulfides in stage II ore samples were analyzed. Moreover, trace elements in seven calcite samples (4 from stage I and 3 from stage II) were analyzed. The ore samples were first crushed to 40–80 mesh for mineral separation (incl. cassiterite, sulfide, and calcite) using standard magnetic and heavy liquid separation techniques, and then handpicked under a binocular microscope to ensure a high level of purity.

3.1. LA-ICP-MS Cassiterite U-Pb Dating

The fracture-/inclusion-free cassiterite samples were mounted in epoxy resin. Before U-Pb dating, cathodoluminescence images of cassiterite were taken using a Zeiss Supra 55 field emission scanning electron coupled with a cathodoluminescence detector at the State Key Laboratory of Isotope Geochemistry, Guangzhou Institute of Geochemistry, Chinese Academy of Sciences (GIGCAS), Guangzhou, China. In situ cassiterite U-Pb dating was analyzed on an Agilent 7900 ICP-MS coupled with a Resonetics Resolution S-155 laser ablation system at the Key Laboratory of Mineralogy and Metallogeny, GIGCAS. The laser ablation spot size was 51 μm . Samples NIST 610 and cassiterite AY-4 [3] were used as the external standards for element and isotope calibration, respectively. Detailed cassiterite U-Pb dating procedures followed [28]. Tera—Wasserburg concordia plotting and weighted

mean age calculations were performed with Isoplot 3.0. Analytical uncertainty for the isotopic ratios and weighted mean $^{206}\text{Pb}/^{238}\text{U}$ age are reported as 1σ and 2σ , respectively.

3.2. Hydrogen-Oxygen Isotope Analyses

Fluid inclusion H-O isotope analyses on sulfides were conducted at the Beijing Research Institute of Uranium Geology, Beijing, China (BRIUG). The selected sulfides (~25 g) samples were first enclosed in a molybdenum tube and then dried for about 12 h at $150\text{ }^{\circ}\text{C}$ under vacuum conditions to eliminate adsorbed air moisture. Subsequently, the samples were heated to about $500\text{ }^{\circ}\text{C}$ in an induction oven until all the gas was released. Oxygen was directly liberated from the separated H_2O from fluid inclusions by reaction with BrF_5 . The resultant oxygen was reacted with graphite rods to produce carbon dioxide. The resultant H_2O was reduced to H_2 by hot zinc at $450\text{ }^{\circ}\text{C}$. The H-O isotope compositions were analyzed on a Finnigan MAT-252 ratio mass spectrometer. The precision were determined by repeated analyses for $\delta^{18}\text{O}$ and δD is $\pm 0.2\text{‰}$ and $\pm 2\text{‰}$, respectively. The O-H isotope data are expressed in ‰ relative to the Vienna Standard Mean Ocean Water (V-SMOW).

3.3. Sulfide Pb and S Isotope Analyses

Sulfide grains separated from stage II ore were dissolved by HNO_3 . The cation exchange resin with 0.5 mol/L HBr was used to separate highly purified Pb. The Pb collected by 6N HCl was evaporated to dryness, leading to PbCl_2 precipitation. The PbCl_2 was then redissolved in distilled water, and the solution was loaded on a single Re-filament. The Pb isotopic ratios were determined by a solid source single-collector mass spectrometer at the BRIUG. The NBS981 and NBS 982 common Pb standards were used to trace instrument mass fractionation (based on repeated analyses). The total standard variations observed in the duplicates (2σ) are generally $<0.1\%$ for $^{206}\text{Pb}/^{204}\text{Pb}$ and $^{207}\text{Pb}/^{204}\text{Pb}$, and 0.3% for $^{208}\text{Pb}/^{204}\text{Pb}$.

Sulfide S isotope ratio was analyzed by the direct oxidation method with a MAT 174 253 mass spectrometer at the BRIUG. GBW 04415 and GBW 04414 were used as standards. The analytical uncertainty for $\delta^{34}\text{S}$ is better than 0.1‰ (2σ).

3.4. Calcite Trace Element Analysis

The analysis was performed at the Guizhou Tongwei Analytical Technology Co. Ltd., Guiyang, China on a Thermal X series 2 equipped with a Cetac ASX-510 Auto Sampler. The calcite powder was dissolved in Teflon bomb with double distilled concentrated HNO_3 -HF (1:4) mixture. The ICP-MS procedures follow those described by [29] with modifications suggested by [30,31]. Data accuracy and precision are better than 10% for trace elements, based on repeated analyses of the USGS standard W-2a.

4. Results

4.1. Cassiterite U-Pb Age

Most cassiterite grains from Beixiang are pale-yellow to colorless and euhedral-subhedral and have apparent oscillatory zonation (Figure 4). Overall, 28 cassiterite grains were analyzed: 7 with large errors were discarded, and the remaining 21 had 0.26–8.28 ppm U (Table 1), yielding a U–Pb concordia lower intercept age of $90.6 \pm 4.5\text{ Ma}$ (MSWD = 2.4, Figure 4).

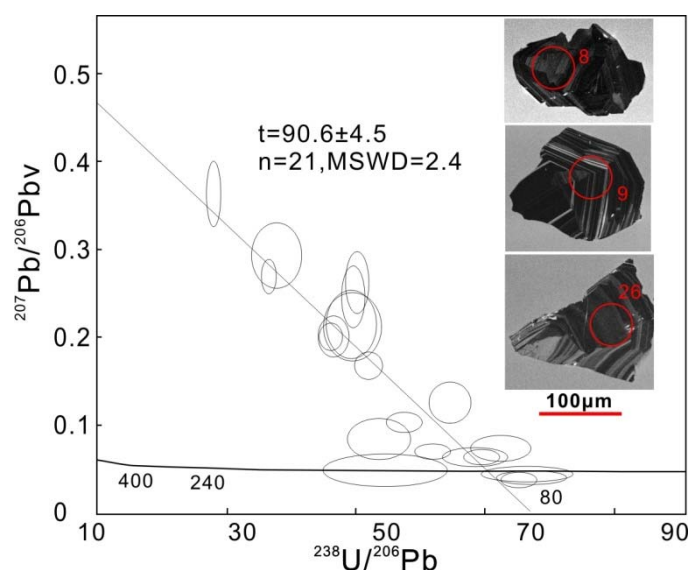


Figure 4. Tera—Wasserburg U—Pb diagram for cassiterites from the Beixiang deposit. Insets show cathodoluminescence images of representative cassiterite samples.

Table 1. LA-ICP-MS U-Pb dating results of cassiterite from the Beixiang deposit.

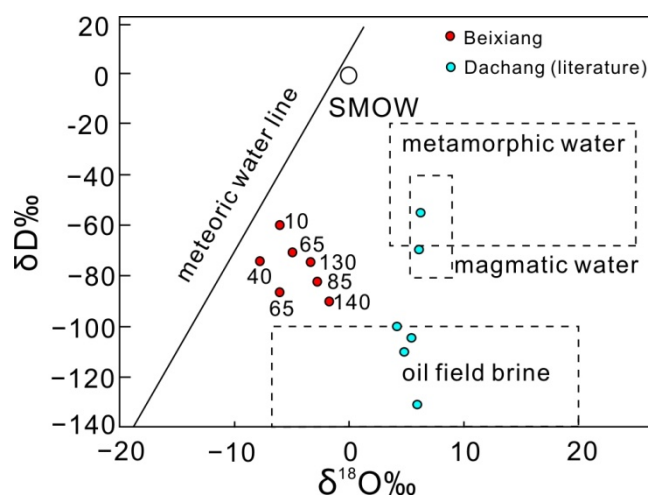
| Spots | U | | Isotopic Ratios | | | | | Age (Ma) | | | | |
|-------|------|-----------------------------------|-----------------|----------------------------------|-----------|----------------------------------|-----------|----------------------------------|-----------|----------------------------------|-----------|--|
| | ppm | $^{207}\text{Pb}/^{206}\text{Pb}$ | 1σ | $^{207}\text{Pb}/^{235}\text{U}$ | 1σ | $^{206}\text{Pb}/^{238}\text{U}$ | 1σ | $^{207}\text{Pb}/^{235}\text{U}$ | 1σ | $^{206}\text{Pb}/^{238}\text{U}$ | 1σ | |
| BX-1 | 2.49 | 0.127473 | 0.016865 | 0.211775 | 0.015879 | 0.015454 | 0.000622 | 195.0 | 13.3 | 98.9 | 3.9 | |
| BX-2 | 2.98 | 0.245726 | 0.028331 | 0.545729 | 0.038940 | 0.020082 | 0.000890 | 442.2 | 25.6 | 128.2 | 5.6 | |
| BX-3 | 1.68 | 0.202196 | 0.018196 | 0.549188 | 0.042739 | 0.021393 | 0.000892 | 444.5 | 28.0 | 136.5 | 5.6 | |
| BX-4 | 2.98 | 0.269112 | 0.015447 | 0.911367 | 0.046302 | 0.027270 | 0.000755 | 657.8 | 24.6 | 173.4 | 4.7 | |
| BX-5 | 1.13 | 0.073391 | 0.013785 | 0.148850 | 0.015674 | 0.013803 | 0.000735 | 140.9 | 13.9 | 88.4 | 4.7 | |
| BX-6 | 4.83 | 0.167807 | 0.012033 | 0.395772 | 0.024276 | 0.019220 | 0.000684 | 338.6 | 17.7 | 122.7 | 4.3 | |
| BX-7 | 2.91 | 0.200031 | 0.013062 | 0.535225 | 0.028003 | 0.021544 | 0.000630 | 435.3 | 18.5 | 137.4 | 4.0 | |
| BX-8 | 4.00 | 0.061977 | 0.007816 | 0.096413 | 0.007968 | 0.014218 | 0.000517 | 93.5 | 7.4 | 91.0 | 3.3 | |
| BX-9 | 4.22 | 0.064102 | 0.008326 | 0.107445 | 0.010686 | 0.014765 | 0.000699 | 103.6 | 9.8 | 94.5 | 4.4 | |
| BX-10 | 0.56 | 0.084976 | 0.016232 | 0.313073 | 0.035072 | 0.018621 | 0.001305 | 276.6 | 27.1 | 118.9 | 8.3 | |
| BX-13 | 3.93 | 0.037967 | 0.005001 | 0.060308 | 0.005639 | 0.013250 | 0.000439 | 59.5 | 5.4 | 84.9 | 2.8 | |
| BX-14 | 1.88 | 0.218892 | 0.025143 | 0.415743 | 0.026767 | 0.019576 | 0.000846 | 353.0 | 19.2 | 125.0 | 5.3 | |
| BX-15 | 2.06 | 0.212901 | 0.029590 | 0.504662 | 0.047633 | 0.020234 | 0.001219 | 414.9 | 32.1 | 129.1 | 7.7 | |
| BX-17 | 1.96 | 0.293382 | 0.028791 | 0.884549 | 0.071624 | 0.026402 | 0.001890 | 643.4 | 38.6 | 168.0 | 11.9 | |
| BX-18 | 2.80 | 0.264391 | 0.026925 | 0.620171 | 0.044104 | 0.019834 | 0.000714 | 490.0 | 27.6 | 126.6 | 4.5 | |
| BX-19 | 3.23 | 0.365046 | 0.027831 | 1.806718 | 0.121156 | 0.035595 | 0.001346 | 1047.9 | 43.8 | 225.5 | 8.4 | |
| BX-20 | 0.26 | 0.049643 | 0.013750 | 0.586841 | 0.129205 | 0.018151 | 0.002472 | 468.8 | 82.7 | 116.0 | 15.7 | |
| BX-23 | 3.92 | 0.102550 | 0.008052 | 0.264331 | 0.017811 | 0.017358 | 0.000606 | 238.2 | 14.3 | 110.9 | 3.8 | |
| BX-25 | 2.82 | 0.070334 | 0.006733 | 0.123064 | 0.008257 | 0.016109 | 0.000577 | 117.8 | 7.5 | 103.0 | 3.7 | |
| BX-26 | 8.28 | 0.043428 | 0.004649 | 0.091692 | 0.017969 | 0.013190 | 0.000814 | 89.1 | 16.7 | 84.5 | 5.2 | |
| BX-28 | 1.95 | 0.043603 | 0.006319 | 0.051303 | 0.003922 | 0.012661 | 0.000619 | 50.8 | 3.8 | 81.1 | 3.9 | |

4.2. Ore-Fluid H-O Isotope Compositions

The fluid inclusion H-O isotope data of stage II sulfides are summarized in Table 2 and illustrated in Figure 5. The stage II ore-forming fluids have $\delta^{18}\text{O}_{\text{H}_2\text{O}} = -2.8$ to -7.8‰ and $\delta\text{D}_{\text{V-SMOW}} = -90.5$ to -59.3‰ . The H-O data points fall among the magmatic water, meteoric water, and oil field brine fields. It is worth noting that the ore-fluids from deeper parts (i.e., lower elevations) of the orebodies fall closer to the meteoric water line, whereas those from shallower parts (i.e., higher elevations) of the orebodies are nearer to the oil field brine (Figure 5).

Table 2. Hydrogen and oxygen isotopic compositions of fluid inclusions from second-stage mineralization sulfide in the Beixiang deposit.

| Sample No. | Location (Depth above Sea Level) | Mineral | $\delta^{18}\text{O}_{\text{V-SMOW}}$ (‰) | $\delta\text{D}_{\text{V-SMOW}}$ (‰) |
|------------|----------------------------------|------------|---|--------------------------------------|
| TWS-01 | No.1 vein, 10 m | sphalerite | −6.1 | −59.3 |
| TWS-02 | No.1 vein, 40 m | pyrite | −7.8 | −73.9 |
| TWS-03 | No.1 vein, 65 m | sphalerite | −4.9 | −71.3 |
| TWS-04 | No.1 vein, 65 m | jamesonite | −6.1 | −87.4 |
| TWS-05 | No.1 vein, 85 m | sphalerite | −3.8 | −82.4 |
| TWS-06 | No.3 vein, 130 m | sphalerite | −3.5 | −74.7 |
| TWS-07 | No.3 vein, 140 m | pyrite | −2.8 | −90.5 |

**Figure 5.** Plot of fluid inclusion H-O isotopes of sulfides from the Beixiang stage II ores. Data near the composition point indicate the sample elevation (meter) above sea level.

4.3. Sulfide S Isotopes

Sulfide S-isotope data (sphalerite, pyrite, and jamesonite) from Beixiang Stage II ore are listed in Table 3. The different sulfides from Beixiang have similar $\delta^{34}\text{S}_{\text{V-CDT}}$ values (−6.2 to −4.0‰), which are lower than those of the Jianzhupo Zn-Sb-Sn-Pb deposit (3.9–8.0‰, avg. 6.1‰) in the Wuxu ore field [32] and the Tongkeng and the Gaofeng deposits (−9.3 to 3.7‰, avg. −2.8‰) in the Dachang ore field (Table 3, [33]).

Table 3. Sulfur isotopic compositions of the Beixiang deposit.

| Deposit/Orefield | Samples | Mineral | $\delta^{34}\text{S}_{\text{V-CDT}}$ (‰) | Average |
|---------------------------------|-------------------------|------------|--|---------|
| Beixiang | TWS-01 | sphalerite | −5.4 | −5.4 |
| | TWS-02 | pyrite | −4.1 | |
| | TWS-03 | sphalerite | −5.0 | |
| | TWS-04 | jamesonite | −5.3 | |
| | TWS-05 | sphalerite | −5.3 | |
| | TWS-06 | sphalerite | −6.2 | |
| | TWS-07 | pyrite | −6.2 | |
| Tongkeng (Dachang ore field) | 68 samples ^a | sulfides | −9.3–3.7 | −2.8 |
| Wuxu ore field | 39 samples ^b | sulfides | 3.9–8.1 | 6.1 |

^a Data from Liang et al., 2008. ^b Data from Liu et al., 2020.

4.4. Sulfide Pb Isotopes

Lead isotopic data of the sphalerite, pyrite, and jamesonite from Beixiang stage II ore are listed in Table 4 and shown in the $^{207}\text{Pb}/^{204}\text{Pb}$ vs. $^{206}\text{Pb}/^{204}\text{Pb}$ plot (Figure 6). The different sulfides have similar Pb isotope compositions, with $^{206}\text{Pb}/^{204}\text{Pb} = 18.515\text{--}18.582$, $^{207}\text{Pb}/^{204}\text{Pb} = 15.413\text{--}15.812$, and $^{208}\text{Pb}/^{204}\text{Pb} = 38.991\text{--}39.292$. The Beixiang sulfides have similar Pb isotopes as those from the Dachang ore field (Figure 6).

Table 4. Pb isotopic compositions of the Beixiang deposit.

| Sample Number | Mineral | $^{206}\text{Pb}/^{204}\text{Pb}$ | $^{207}\text{Pb}/^{204}\text{Pb}$ | $^{208}\text{Pb}/^{204}\text{Pb}$ |
|---------------|------------|-----------------------------------|-----------------------------------|-----------------------------------|
| TWS-01 | sphalerite | 18.516 | 15.413 | 39.009 |
| TWS-02 | pyrite | 18.545 | 15.760 | 39.121 |
| TWS-03 | sphalarite | 18.532 | 15.739 | 39.058 |
| TWS-04 | jamesonite | 18.582 | 15.812 | 39.292 |
| TWS-05 | sphalerite | 18.520 | 15.720 | 38.989 |
| TWS-06 | sphalerite | 18.526 | 15.721 | 39.007 |
| TWS-07 | pyrite | 18.515 | 15.723 | 38.991 |

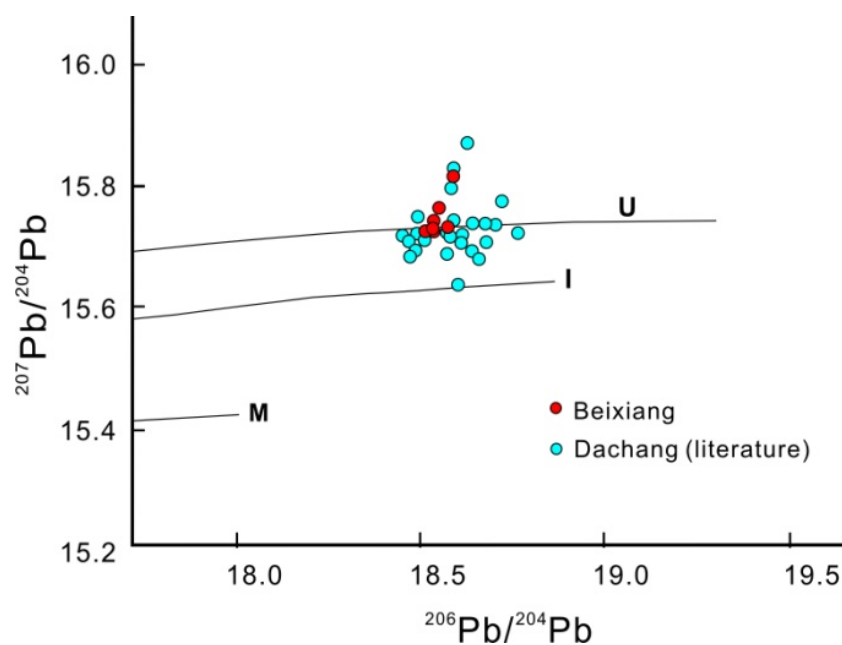


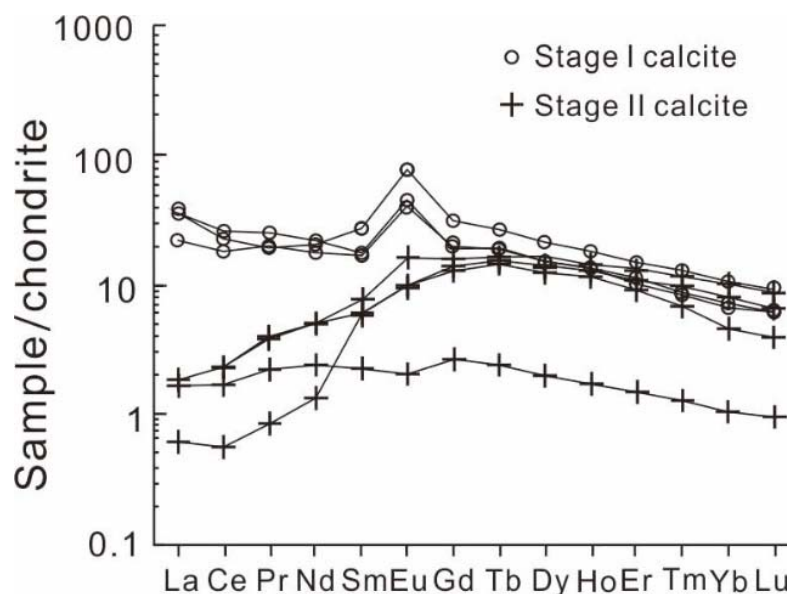
Figure 6. $^{206}\text{Pb}/^{204}\text{Pb}$ vs. $^{207}\text{Pb}/^{204}\text{Pb}$ plot of the Beixiang deposit. Plumbotectonic framework trends are plotted for reference (U: upper crust, I: orogen, M: mantle [34]).

4.5. Calcite REE Compositions

Calcite REE data are listed in Table 5 and plotted in Figure 7. Calcite samples from stage I and II ores have different REE chondrite-normalized patterns and Eu anomalies. Stage I calcite has total $\Sigma\text{REE} = 49.32\text{--}54.96$ ppm, $(\text{La}/\text{Yb})_{\text{N}} = 2.15\text{--}4.91$, and positive Eu anomaly ($\delta\text{Eu}: 2.06\text{--}2.68$). Stage II calcite has much lower ΣREE (4.96–19.95 ppm) than its stage I counterpart. Stage II calcite is characterized by flattened chondrite-normalized REE patterns ($(\text{La}/\text{Yb})_{\text{N}} = 0.14\text{--}1.57$) with weak positive-to-negative Eu anomaly ($\delta\text{Eu}: 0.84\text{--}1.57$) (Figure 7).

Table 5. Calcite REE concentration of early and second-stage mineralization from the Beixiang deposit.

| Element (ppm) | Stage I Mineralization | | | | Stage II Mineralization | | | |
|----------------------|------------------------|---------|---------|---------|-------------------------|---------|---------|--|
| | BX-WL01 | BX-WL03 | BX-WL04 | BX-WL05 | BX-WL06 | BX-WL07 | BX-WL08 | |
| La | 9.11 | 5.24 | 8.15 | 0.39 | 0.43 | 0.41 | 0.15 | |
| Ce | 15.60 | 11.10 | 13.60 | 1.04 | 1.38 | 1.37 | 0.35 | |
| Pr | 2.39 | 1.90 | 1.92 | 0.21 | 0.37 | 0.36 | 0.08 | |
| Nd | 10.12 | 9.22 | 8.01 | 1.12 | 2.44 | 2.29 | 0.64 | |
| Sm | 2.58 | 4.12 | 2.69 | 0.35 | 1.22 | 0.98 | 0.92 | |
| Eu | 2.59 | 4.51 | 2.28 | 0.12 | 0.94 | 0.59 | 0.53 | |
| Gd | 3.66 | 6.44 | 4.26 | 0.55 | 2.96 | 2.48 | 3.38 | |
| Tb | 0.67 | 0.99 | 0.69 | 0.09 | 0.65 | 0.56 | 0.55 | |
| Dy | 4.02 | 5.44 | 3.79 | 0.51 | 4.17 | 3.50 | 3.12 | |
| Ho | 0.79 | 1.00 | 0.70 | 0.10 | 0.87 | 0.72 | 0.63 | |
| Er | 1.94 | 2.44 | 1.67 | 0.25 | 2.25 | 1.83 | 1.47 | |
| Tm | 0.25 | 0.32 | 0.22 | 0.03 | 0.31 | 0.25 | 0.17 | |
| Yb | 1.30 | 1.75 | 1.19 | 0.18 | 1.73 | 1.34 | 0.79 | |
| Lu | 0.17 | 0.23 | 0.16 | 0.02 | 0.23 | 0.18 | 0.10 | |
| ∑REE | 54.96 | 54.70 | 49.32 | 4.96 | 19.95 | 16.87 | 12.88 | |
| (La/Yb) _N | 4.97 | 2.15 | 4.91 | 1.57 | 0.18 | 0.22 | 0.14 | |
| (La/Sm) _N | 2.25 | 0.82 | 1.96 | 0.73 | 0.23 | 0.27 | 0.10 | |
| (Gd/Lu) _N | 2.73 | 3.40 | 3.33 | 2.85 | 1.60 | 1.71 | 4.18 | |
| δEu | 2.58 | 2.68 | 2.06 | 0.84 | 1.51 | 1.16 | 0.92 | |

**Figure 7.** Plot of calcite REE patterns for the Beixiang stage I and II mineralization. Chondrite values are from reference [35].

5. Discussion

5.1. Mineralization Timing of the Beixiang Deposit and the Danchi Ore Belt

Previous cassiterite U-Pb and zircon U-Pb dating showed that many granite-related Sn deposits in the Danchi ore belt, such as the Mangchang ore field in the north and the Dachang ore field in the middle of the ore belt were formed during 89.1~95.4 Ma [11,12,14,25].

Our cassiterite U-Pb age (90.6 ± 2.4 Ma, Figure 4) indicates that the Beixiang deposit in the southern part of the ore belt was also formed in the early Late Cretaceous period. The age of Beixiang Sn ore is similar to the other granite-related Sn ores in the Danchi ore belt,

indicating that the Sn-polymetallic mineralization of the entire Danchi ore belt occurred during the Late Cretaceous period.

5.2. Sources of the Stage II Sb-Pb-Zn Mineralization

5.2.1. Sources of Ore-Forming Elements

Sulfide minerals contain low U-Th concentrations and could thus maintain their primary Pb isotope compositions and represent that of the Pb sources [34]. The sulfides from the Beixiang stage II ore have their Pb isotopes falling along/above the upper crustal growth curve (Figure 6, [34]) indicating that the Pb was derived from preexisting evolved crustal rocks, either the ore hosting strata or the Proterozoic metamorphic basement.

Sulfide S-isotopes ($\delta^{34}\text{S}$) are widely used to reveal the ore material source [36] and can reflect the ore-fluid S-isotope ratios in sulfide-dominated deposits [37], as in the case of Beixiang, where sulfates are absent. The sulfides of stage II ore have narrow-range $\delta^{34}\text{S}_{\text{V-CDT}}$ (-4.0 to -6.2% , avg. -5.4%) that are slightly lower than that of magmatic sulfur ($0 \pm 3\%$) [37,38]. The S isotope features, together with the fact that the ore-forming fluids of stage II were derived from oil field brine and meteoric water (detailed in Section 5.2.2), suggest that the sulfur of Beixiang stage II ore was derived from local strata.

Based on the sulfide Pb and S isotopes, it is reasonable to suggest that the Pb in stage II mineralization was mainly derived from the local strata.

5.2.2. Fluid Sources of Stage II Sb-Pb-Zn Mineralization

The stage II ores have H-O isotope compositions that fall among the meteoric water line, magmatic water, metamorphic water, and oil field brine on the $\delta^{18}\text{O}_{\text{H}_2\text{O}}$ vs. $\delta\text{D}_{\text{V-SMOW}}$ plot (Figure 5). The ore-fluid H-O isotope compositions were likely caused by the mixing of meteoric, metamorphic, magmatic, and oil field brine. Given that no intensive metamorphism occurred after the Caledonian orogeny (460–420 Ma) in South China [39], a metamorphic fluid source was unlikely for the stage II mineralization. The ore-fluid δD values can be significantly lowered through reacting with organic matter [40]. Based on the linear $\delta^{18}\text{O}_{\text{H}_2\text{O}}$ vs. $\delta\text{D}_{\text{V-SMOW}}$ variation between the meteoric water line and oil field brine end-members (Figure 5), we suggest the fluid was sourced from the mixing of oilfield brine and meteoric water with minor magmatic water.

The ore-fluid $\delta\text{D}_{\text{V-SMOW}}$ and $\delta^{18}\text{O}_{\text{H}_2\text{O}}$ values show negative and positive correlation with mineralization depth, respectively (Figure 8). These features suggest that the ore fluid of the shallower-level mineralization contains more oil field brine than that of deeper-level mineralization. Such variation in the amount of oil field brine was possibly caused by the circulation of meteoric water, which entered the local strata downward at first, then migrated upward and mixed with more oil field brine at the shallower level. Since the Sb-Pb-Zn assemblage is commonly enriched in oil field brine [41,42], we suggest that oil field brine should have promoted these elements' enrichment in stage II mineralization.

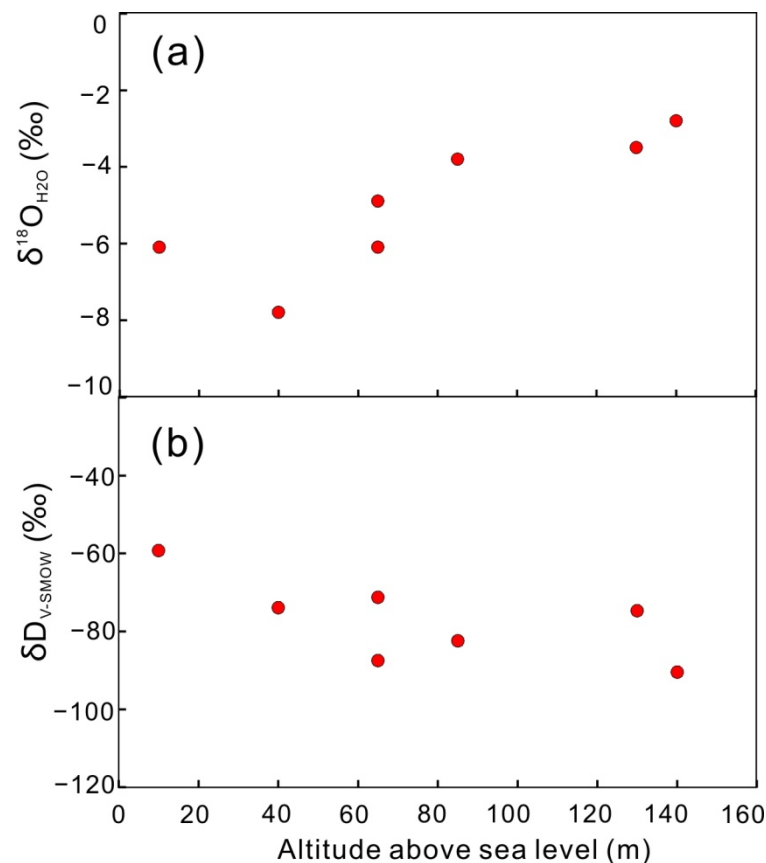


Figure 8. Plot of H-O isotopes vs. altitude.

5.3. Distinct Source for the Stage I Zn-Sn Ore from the Stage II Sb-Pb-Zn Ore

Hydrothermal calcite can readily accommodate trivalent REE in its mineral lattice, resulting in their higher enrichment in calcite than in fluid [43–45], and thus calcite REE signature could be used to trace ore-forming processes [45–47]. Europium anomalies in Ca-minerals, such as calcite and fluorite, can indicate the origin of the ore fluid [48]. The ionic radius of Eu³⁺ (0.95 Å) is similar to Ca²⁺ (1.00 Å) in calcite, whereas the radius of Eu²⁺ (1.17 Å) is larger than Ca²⁺, and thus divalent Eu would be rejected by the calcite lattice [49].

Stage II calcite is characterized by upward-convex REE patterns with weak positive-to-negative Eu anomalies, similar to the calcite from Carlin-type gold deposits in SW China [50]. Moreover, stage II calcite has a similar composition as that of the calcite in alpine fissure and limestone on the Yb/La vs. Yb/Ca plot (Figure 9, [48]). These suggest that the stage II ore fluid was mainly sourced from basin brine or circulated meteoric water, which is consistent with the conclusion from signatures of H-O isotope compositions.

Stage I calcite is characterized by strong positive δEu anomalies (Eu_N/Eu* = 2.06–2.68) with high (La/Yb)_N (2.15–4.91) and REE contents (49.32–54.96 ppm). Given that REE³⁺ ions are more compatible in the calcite lattice [47,51], these REE differences between stage I and II calcite indicate that their ore fluids have distinct sources. Stage I calcite has a positive Eu anomaly, indicating that the early ore fluid is characterized by high Eu content. The positive Eu anomalies likely reflect REE addition by the alteration of feldspar, as feldspars are commonly Eu-rich [48]. Since basement rocks in Guangxi comprise plagioclase-poor, low-grade metamorphic rocks such as slate and schist [23,52], they were unlikely the source. On the Yb/La vs. Yb/Ca plot (Figure 9), stage I calcite is located near the carbonatite field [48], showing magmatic affinity. Since granites are widely occurring in the region and usually plagioclase-rich, we suggested that the Sn-Zn ore fluids were likely related to granite greisenization, as supported by the local

presence of marble in the ore field and the similar mineral assemblage (i.e., cassiterite-pyrite-arsenopyrite \pm sulfide) of this stage to those in the Dachang Sn-polymetallic deposit [10]. Moreover, 99% of Sn deposits in the world are granite-related [53] and most Sn-related granites underwent greisenization; the greisenization-derived fluids should be Sn-rich and generate the Stage I Zn-Sn mineralization.

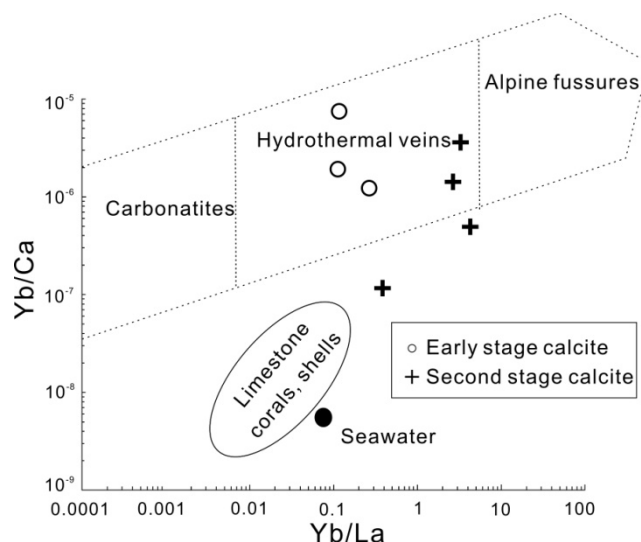


Figure 9. Plot of Yb/La vs. Yb/Ca in calcite. The areas of different types of calcite are from reference [48].

Overall, we suggest that unlike the stage II Sb-Pb-Zn ore fluids sourced from mixing of oil field brine and meteoric water, the stage I Sn-Zn ore fluids, as well as the Sn and Zn, were sourced from granitic magma.

5.4. Genesis of the Beixiang Deposit and Implications

Granites and associated Sn deposits are well developed throughout the Danchi ore belt (Figure 1). Although there are no granite intrusions observed in the Beixiang deposit, the local presence of marble in the ore field, as well as the magmatic affinity of the stage I ore fluids consistently suggest that there should be a blind granite at depth, which provided materials and heat for the mineralization in the Beixiang ore deposit.

Previous works proposed that the late Yanshanian Sn-polymetallic deposits in SW China-western Myanmar were triggered by Neo-Tethys subduction and roll-back [12]. Consequently, we propose a model for the Beixiang Sb-Pb-Zn-Sn metallogeny (Figure 10): (1) the subduction of the Neo-Tethys Plate might have triggered Sn-bearing granitic magmatism with intrusions emplaced at depth under the Beixiang ore field; (2) the Sn-bearing granites might have undergone greisenization and released ore-forming fluids that moved upward to fracture zones and formed stage I Zn-Sn mineralization; and (3) the granitic magma and the related ore-forming fluid heated and triggered the circulation of meteoric water, which mixed with oil field brine at the shallow levels and then formed stage II Sb-Pb-Zn mineralization deposited at the top and around the first stage mineralization. Multi-stage mineralization with multiple sources of materials is the key factor for the co-enrichment of Sn-Sb-Pb-Zn within the Beixiang ore field.

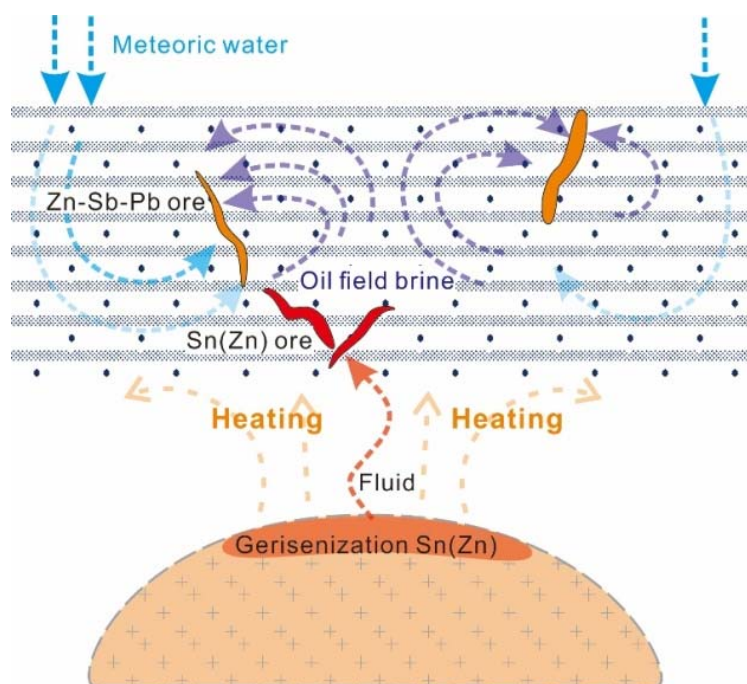


Figure 10. Schematic model of the Beixiang Sn polymetallic mineralization.

Given that the Beixiang stage I Sn-Zn ore should be granite-related and greisen-type Sn mineralization usually occurred at the top of granite, we suggest that the deep part of the Beixiang ore field has great prospecting potential for greisen-type Sn-Zn ores.

5.5. Processes for Sb-Pb Enrichment in the Danchi Belt

Granite Sn-W deposits are usually Zn-rich and Pb-poor because the source rocks of granitic magmas are commonly strongly weathered, which could cause Pb loss by feldspar decomposition [1,2]. Studies on the granites of the Cornubian Batholith indicated that Sb is not enriched by fractionation in the granites [5]. Although some Sn deposits in the Central Andean Sn belt contain late Sb mineralization [6], deposits that principally contained metals of Sn-Sb ± Pb have rarely been found so far.

The Danchi ore belt is characterized by enrichments of both Sn-Zn and Sb-Pb [11,16,22,25]. For example, the giant Gaofeng Sn-polymetallic deposit in the Dachang ore field has 0.34 Mt Sn @ 1.9%, 1.5 Mt Zn @ 12.4%, 0.65 Mt Sb @ 5.78%, and 0.79 Mt Pb @ 6.55% [54], whereas the Jianzhupo deposit in Wuxu ore field has a reserve of 224 kt Zn, 136 kt Sb, and 84 kt Pb, with minor Sn endowment at depth [16].

Our data indicate that the ore-forming fluids for Beixiang stage I Sn-Zn ore was granite-related and Sn-rich, and for stage II ore was oil field brine-related and Sb-Pb-Zn-rich. The Cretaceous granites also generated the Sn enrichment in Dachang and Wuxu ore fields. Bitumen was found in ore deposits in the Wuxu [16] and Dachang ore fields [19], which fingerprints the oil field brine. The ore-fluid H-O isotope features of deposits in the Dachang and Wuxu ore fields are characterized by a large variation of δD values and located between oil field brine to magmatic water or meteoric water (Figure 5), also suggesting oil field brine involvement during their mineralization.

Our data also revealed that the local strata should have contributed Pb to stage II ore. The $\delta^{34}S_{V-CDT}$ average value (-5.4‰) of Beixiang stage II sulfide is lower than those of other deposits in the Danchi ore belt, such as the giant Tongkeng Sn-polymetallic deposit (-7.9 to -2.6‰ , avg. -3.34‰) in the Dachang ore field [55] and the Jianzhupo deposit in the Wuxu ore field (avg. 6.1‰) (Figure 1a). Pyrite from unaltered sedimentary rocks in the Wuxu ore field (Figure 1a) has relatively high $\delta^{34}S_{V-CDT}$ value ($\sim 10.1\text{‰}$), which may cause relatively high $\delta^{34}S_{V-CDT}$ values in Jianzhupo deposit. This suggests that the sulfur isotope compositions of ores in the Danchi ore belt are related to the sulfur compositions of the local

ore-hosting strata, which should be the dominating sulfur-source. Moreover, the Dachang deposits have similar Pb isotope compositions [55,56] as the Beixiang stage II ore (Figure 6), suggesting that the Pb in the former was likely derived from a similar local strata. The oil field brine is commonly Sb-Pb-Zn-enriched [41,42], suggesting that the oil field brine or the circulating meteoric water could extract Sb-Pb-Zn from local strata. We therefore suggest that multiple sources of ore-forming fluids and materials (i.e., granite-related and oilfield brine-related) are likely the key factors in the generation of the deposits rich in Sn-Sb-Zn-Pb in the Danchi belt.

6. Conclusions

1. The Beixiang Zn-Pb-Sb-Sn mineralization was dated by U-Pb in cassiterite at 90.6 ± 4.5 Ma, coeval with the other deposits in the Danchi Sn-polymetallic ore belt, suggesting that a regional mineralization event occurred during the Late Cretaceous period.
2. The Beixiang stage I Zn-Sn and the stage II Pb-Zn-Sb ore fluids were sourced from the local granitic magmatism and a mixture of oil field brine and meteoric water, respectively.
3. The Danchi ore belt with the Sn-Zn-Sb-Pb assemblage was likely attributed to the co-mineralization of granite-derived Sn-Zn-rich and oil field brine and circulation of meteoric water-derived Sb-Pb-Zn-rich ore fluids.

Author Contributions: Conceptualization, Z.L.; Data curation, J.L. and J.Z.; Funding acquisition, J.W., J.Z. and H.L.; Methodology, J.Z.; Project administration, Z.L.; Writing – original draft, J.W., M.Z., W.H., J.L., J.Z. and H.L. All authors have read and agreed to the published version of the manuscript.

Funding: This project was financially supported by the NSFC (42062007, 42002080, 41772065).

Data Availability Statement: Not applicable.

Acknowledgments: The anonymous reviewers are thanked for greatly improving the manuscript through their thoughtful and thorough reviews. Staffs from the Beixiang Mining Co. Ltd. are thanked for the field assistance.

Conflicts of Interest: The authors declare no conflict of interest.

References

1. Romer, R.L.; Kroner, U. Sediment and weathering control on the distribution of Paleozoic magmatic tin-tungsten mineralization. *Miner. Depos.* **2015**, *50*, 327–338. [[CrossRef](#)]
2. Romer, R.L.; Kroner, U. Phanerozoic tin and tungsten mineralization-Tectonic controls on the distribution of enriched protoliths and heat sources for crustal melting. *Gondwana Res.* **2016**, *31*, 60–95. [[CrossRef](#)]
3. Yuan, S.D.; Peng, J.T.; Hao, S.; Li, H.M.; Geng, J.Z.; Zhang, D.L. In situ LA-MC-ICP-MS and ID-TIMS U-Pb geochronology of cassiterite in the giant Furong tin deposit, Hunan Province, South China: New constraints on the timing of tin-polymetallic mineralization. *Ore Geol. Rev.* **2011**, *43*, 235–242. [[CrossRef](#)]
4. Yuan, S.D.; Williams-Jones, A.E.; Romer, R.L.; Zhao, P.L.; Mao, J.W. Protolith-Related Thermal Controls on the Decoupling of Sn and W in Sn-W Metallogenic Provinces: Insights from the Nanling Region, China. *Econ. Geol.* **2019**, *114*, 1005–1012. [[CrossRef](#)]
5. Simons, B.; Andersen, J.C.O.; Shail, R.K.; Jenner, F.E. Fractionation of Li, Be, Ga, Nb, Ta, In, Sn, Sb, W and Bi in the peraluminous Early Permian Variscan granites of the Cornubian Batholith: Precursor processes to magmatic-hydrothermal mineralisation. *Lithos* **2017**, *278*, 491–512. [[CrossRef](#)]
6. Sugaki, A.U.H.; Shimada, N.; Kuscchi, I.; Kitakaze, A.; Hayashi, K.; Kojima, S.; Sanjines, O.V. *Geological Study on the Polymetallic Ore Deposits in the Potshi District, Bolivia*; The Science Reports of the Tohoku University: Sendai, Japan, 1983; pp. 409–460.
7. Sillitoe, R.H.; Lehmann, B. Copper-rich tin deposits. *Miner. Depos.* **2022**, *57*, 1–11. [[CrossRef](#)]
8. Peng, J.T.; Hu, R.Z.; Lin, Y.X.; Zhao, J.H. Sm-Nd isotope dating of hydrothermal calcites from the Xikuangshan antimony deposit, Central Hunan. *Chin. Sci. Bull.* **2002**, *47*, 1134–1137. [[CrossRef](#)]
9. Zhang, T.Y.; Li, C.Y.; Sun, S.J.; Hao, X.L. Geochemical characteristics of antimony and genesis of antimony deposits in South China. *Acta Petrol. Sin.* **2020**, *36*, 44–54. (In Chinese with English Abstract).
10. Fu, M.; Kwak, T.A.P.; Mernagh, T.P. Fluid Inclusion Studies of Zoning in the Dachang Tin-Polymetallic Ore Field, Peoples-Republic-of-China. *Econ. Geol.* **1993**, *88*, 283–300. [[CrossRef](#)]

11. Guo, J.; Zhang, R.Q.; Sun, W.D.; Ling, M.X.; Hu, Y.B.; Wu, K.; Luo, M.N.; Zhang, L.C. Genesis of tin-dominant polymetallic deposits in the Dachang district, South China: Insights from cassiterite U-Pb ages and trace element compositions. *Ore Geol. Rev.* **2018**, *95*, 863–879. [[CrossRef](#)]
12. Huang, W.T.; Liang, H.Y.; Zhang, J.; Wu, J.; Chen, X.L.; Ren, L. Genesis of the Dachang Sn-polymetallic and Baoshan Cu ore deposits, and formation of a Cretaceous Sn-Cu ore belt from southwest China to western Myanmar. *Ore Geol. Rev.* **2019**, *112*, 103030. [[CrossRef](#)]
13. Liang, T.; Wang, D.H.; Hou, K.J.; Li, H.Q.; Huang, H.M.; Cai, M.H.; Wang, D.M. LA-MC-ICP-MS zircon U-Pb dating of Longxianggai pluton in Dachang of Guangxi and its geological significance. *Acta Petrol. Sin.* **2011**, *27*, 1624–1636, (In Chinese with English Abstract).
14. Wu, J.; Yuan, H.W.; Gan, N.J.; Wei, S.C.; Liao, J.; Zhang, J.; Liang, H.Y. Source characteristics of magmatic rocks and zircon U-Pb age in the Mangchang ore field, Danchi metallogenic belt, Guangxi. *Acta Petrol. Sin.* **2020**, *36*, 1586–1596, (In Chinese with English Abstract).
15. Zaw, K.; Peters, S.G.; Cromie, P.; Burrett, C.; Hou, Z.Q. Nature, diversity of deposit types and metallogenic relations of South China. *Ore Geol. Rev.* **2007**, *31*, 3–47. [[CrossRef](#)]
16. Zhang, J.; Huang, W.T.; Liang, H.Y.; Wu, J.; Chen, X.L. Genesis of the Jianzhupo Sb-Pb-Zn-Ag deposit and formation of an ore shoot in the Wuxu ore field, Guangxi, South China. *Ore Geol. Rev.* **2018**, *102*, 654–665. [[CrossRef](#)]
17. Zhang, R.H.; Zhang, X.T.; Hu, S.M. The role of vapor in the transportation of tin in hydrothermal systems: Experimental and case study of the Dachang deposit, China. *J. Volcanol. Geotherm. Res.* **2008**, *173*, 313–324. [[CrossRef](#)]
18. Zhao, H.; Su, W.C.; Shen, N.P.; Xie, P.; Cai, J.L.; Gan, W.Z. Fluid inclusion study of the Gaofeng tin-polymetallic deposit in the Dachang ore field, Guangxi, China. *Acta Petrol. Sin.* **2018**, *34*, 3553–3566, (In Chinese with English Abstract).
19. Cai, M.H.; Mao, J.W.; Ting, L.; Pirajno, F.; Huang, H.L. The origin of the Tongkeng-Changpo tin deposit, Dachang metal district, Guangxi, China: Clues from fluid inclusions and He isotope systematics. *Miner. Depos.* **2007**, *42*, 613–626.
20. Cai, M.H.; Peng, Z.N.; Hu, Z.S.; Li, Y. Zn, He-Ar and Sr-Nd isotopic compositions of the Tongkeng Tin-polymetallic ore deposit in south China: Implication for ore genesis. *Ore Geol. Rev.* **2020**, *124*, 103605. [[CrossRef](#)]
21. Jiang, S.Y.; Han, F.; Shen, J.Z.; Palmer, M.R. Chemical and Rb-Sr, Sm-Nd isotopic systematics of tourmaline from the Dachang Sn-polymetallic ore deposit, Guangxi Province, PR China. *Chem. Geol.* **1999**, *157*, 49–67. [[CrossRef](#)]
22. Wu, J.; Nong, S.H.; Huang, W.T.; Zhang, J.; Liang, H.Y.; Yuan, J.T.; Ling, C. Geological and geochemical characteristic of Sb-Au and Pb-Zn-Sb mineralization and complex mineralization in the Sanpaidong ore district, Wuxu ore field, Guangxi. *Acta Petrol. Sin.* **2018**, *34*, 1327–1334, (In Chinese with English Abstract).
23. Huang, W.T.; Wu, J.; Liang, H.Y.; Zhang, J.; Ren, L.; Chen, X.L. Ages and genesis of W-Sn and Ta-Nb-Sn-W mineralization associated with the Limu granite complex, Guangxi, China. *Lithos.* **2020**, *352*, 105321. [[CrossRef](#)]
24. Guo, J.; Wu, K.; Seltmann, R.; Zhang, R.Q.; Ling, M.; Li, C.Y.; Sun, W.D. Unraveling the link between mantle upwelling and formation of Sn-bearing granitic rocks in the world-class Dachang tin district, South China. *Geol. Soc. Am. Bull.* **2022**, *134*, 1043–1064. [[CrossRef](#)]
25. Wang, D.H.; Chen, Y.C.; Chen, W.; Sang, H.Q.; Li, H.Q.; Lu, Y.F.; Lin, Z.M. Dating of the Dachang superlarge tin-polymetallic deposit in Guangxi and its implication for the genesis of the No. 100 orebody. *Acta Geol. Sin.* **2004**, *78*, 452–458, (In Chinese with English Abstract).
26. Chi, Z.D.; Zhang, Z.Q.; He, F. Geological Characteristics and Prospecting Indicators of the Beixiang Pb-Zn-Sn Deposit in Hechi of Guangxi. *Geol. Rev.* **2017**, *63*, 181–182, (In Chinese with English Abstract).
27. Qin, L.Y.; He, G.C.; Qin, D.X. Metallogenic geological conditions and prospecting potential evaluation of Ag polymetallic deposit in Beixiang, Guangxi. *Miner. Resour. Geol.* **2008**, *22*, 145–149, (In Chinese with English Abstract).
28. Liu, X.; Vinograd, V.L.; Lu, X.C.; Leonenko, E.V.; Eremin, N.N.; Wang, R.C.; Winkler, B. Thermodynamics of mixing in an isostructural solid solution: Simulation methodologies and application to the rutile-cassiterite system. *Am. Mineral.* **2016**, *101*, 1197–1206. [[CrossRef](#)]
29. Eggins, S.M.; Woodhead, J.D.; Kinsley, L.P.J.; Mortimer, G.E.; Sylvester, P.; McCulloch, M.T.; Hergt, J.M.; Handler, M.R. A simple method for the precise determination of ≥ 40 trace elements in geological samples by ICPMS using enriched isotope internal standardisation. *Chem. Geol.* **1997**, *134*, 311–326. [[CrossRef](#)]
30. Kamber, B.S.; Greig, A.; Schoenberg, R.; Collerson, K.D. A refined solution to Earth's hidden niobium: Implications for evolution of continental crust and mode of core formation. *Precamb. Res.* **2003**, *126*, 289–308. [[CrossRef](#)]
31. Li, B.P.; Greig, A.; Zhao, J.X.; Collerson, K.D.; Quan, K.S.; Meng, Y.H.; Ma, Z.L. ICP-MS trace element analysis of Song dynasty porcelains from Ding, Jiexiu and Guantai kilns, north China. *J. Archaeol. Sci.* **2005**, *32*, 251–259. [[CrossRef](#)]
32. Liu, T.T.; Zhu, C.W.; Wang, D.P.; Zhang, S.G.; Zhang, Q.B. Genesis of the Jianzhupo Pb-Zn-Sb polymetallic deposit in the Wuxu ore field, Guangxi province: Constraints from sulfur isotopes of sulfides and trace elements compositions of sphalerites. *Bull. Mineral. Petrol. Geochem.* **2020**, *39*, 646–662, (In Chinese with English Abstract).
33. Cai, M.H.; Liang, T.; Peng, Z.A.; Fan, S. *Geology and Metallogenesis of the Dachang Ore Field*; Geological Publishing House: Beijing, China, 2014; (In Chinese with English Abstract).
34. Zartman, R.E.; Doe, B.R. Plumbotectonics—The Model. *Tectonophysics* **1981**, *75*, 135–162. [[CrossRef](#)]
35. Sun, S.S.; McDonough, W.F. Chemical and isotopic systematics of oceanic basalts: Implications for mantle composition and processes. *Geol. Soc. Spec. Publ.* **1989**, *42*, 313–345. [[CrossRef](#)]

36. Ohmoto, H. Systematics of Sulfur and Carbon Isotopes in Hydrothermal Ore-Deposits. *Econ. Geol.* **1972**, *67*, 551–578. [[CrossRef](#)]
37. Rye, R.O.; Ohmoto, H. Sulfur and Carbon Isotopes and Ore Genesis—Review. *Econ. Geol.* **1974**, *69*, 826–842. [[CrossRef](#)]
38. Ohmoto, H. Stable Isotope Geochemistry of Ore-Deposits. *Rev. Mineral.* **1986**, *16*, 491–559.
39. Shu, L.S. An analysis of principal features of tectonic evolution in South China Block. *Geol. Bull. China* **2012**, *31*, 1035–1053, (In Chinese with English Abstract).
40. Gleeson, S.A.; Wilkinson, J.J.; Boyce, A.J.; Fallick, A.E.; Stuart, F.M. The occurrence and wider implications of anomalously low delta D fluids in quartz veins, South Cornwall, England. *Chem. Geol.* **1999**, *160*, 161–173. [[CrossRef](#)]
41. Mu, L.; Hu, R.Z.; Bi, X.W.; Tang, Y.Y.; Lan, T.G.; Lan, Q.; Zhu, J.; Peng, J.; Oyebamiji, A. New Insights into the Origin of the World-Class Jinding Sediment-Hosted Zn-Pb Deposit, Southwestern China: Evidence from LA-ICP-MS Analysis of Individual Fluid Inclusions. *Econ. Geol.* **2021**, *116*, 883–907. [[CrossRef](#)]
42. Wilkinson, J.J.; Stoffell, B.; Wilkinson, C.C.; Jeffries, T.E.; Appold, M.S. Anomalously Metal-Rich Fluids Form Hydrothermal Ore Deposits. *Science* **2009**, *323*, 764–767. [[CrossRef](#)]
43. Debruyne, D.; Hulsbosch, N.; Muchez, P. Unraveling rare earth element signatures in hydrothermal carbonate minerals using a source-sink system. *Ore Geol. Rev.* **2016**, *72*, 232–252. [[CrossRef](#)]
44. Tanaka, K.; Kawabe, I. REE abundances in ancient seawater inferred from marine limestone and experimental REE partition coefficients between calcite and aqueous solution. *Geochim. J.* **2006**, *40*, 425–435. [[CrossRef](#)]
45. Zhong, S.J.; Mucci, A. Partitioning of Rare-Earth Elements (Rees) between Calcite and Seawater Solutions at 25-Degrees-C and 1 Atm, and High Dissolved Ree Concentrations. *Geochim. Cosmochim. Acta* **1995**, *59*, 443–453. [[CrossRef](#)]
46. Kalliomaki, H.; Wagner, T.; Fusswinkel, T.; Schultze, D. Textural evolution and trace element chemistry of hydrothermal calcites from Archean gold deposits in the Hattu schist belt, eastern Finland: Indicators of the ore-forming environment. *Ore Geol. Rev.* **2019**, *112*, 103006. [[CrossRef](#)]
47. Perry, E.; Gysi, A.P. Hydrothermal calcite-fluid REE partitioning experiments at 200 degrees C and saturated water vapor pressure. *Geochim. Cosmochim. Acta* **2020**, *286*, 177–197. [[CrossRef](#)]
48. Moeller, P.; Morteani, G. *On the Geochemical Fractionation of Rare Earth Elements during the Formation of Ca-Minerals and Its Application to the Problems of Genesis for Ore Deposit*; Pascal and Francis: Athens, Greece, 1983.
49. Lakshtanov, L.Z.; Stipp, S.L.S. Experimental study of europium (III) coprecipitation with calcite. *Geochim. Cosmochim. Acta* **2004**, *68*, 819–827. [[CrossRef](#)]
50. Su, W.C.; Hu, R.Z.; Xia, B.; Xia, Y.; Liu, Y.P. Calcite Sm-Nd isochron age of the Shuiyindong Carlin-type gold deposit, Guizhou, China. *Chem. Geol.* **2009**, *258*, 269–274. [[CrossRef](#)]
51. Shannon, R.D. Revised Effective Ionic-Radii and Systematic Studies of Interatomic Distances in Halides and Chalcogenides. *Acta Crystallogr. Sect. A* **1976**, *32*, 751–767. [[CrossRef](#)]
52. Huang, W.T.; Liang, H.Y.; Ren, L.; Chen, X.L.; Zhang, J.; Li, K.X. Protolith-controlled superposition of Sn-(W) and Cu-Mo mineralization: Examples from the Jurassic and Cretaceous granite-related mineralization in the coastal region of southeastern China. *Lithos* **2021**, *380*, 105816. [[CrossRef](#)]
53. Lehmann, B. Formation of tin ore deposits: A reassessment. *Lithos* **2021**, *402*, 105756. [[CrossRef](#)]
54. Zhang, J.; Huang, W.T.; Chen, X.L.; Wu, J.; Ren, L.; Liang, H.Y.; Chen, L. Different Geochemical Characteristics and Genetic Link between Sn-polymetallic Deposit and Skarn Zn-Cu Deposit in the Dachang Ore Field, Guangxi. *Geotecton. Metallog.* **2019**, *43*, 1186–1199, (In Chinese with English Abstract).
55. Liang, T.; Wang, D.H.; Cai, M.H.; Chen, Z.Y.; Guo, C.; Huang, H.M. Sulfur and Lead Isotope Composition Tracing for the Sources of Ore-Forming Material in Dachang Tin-Polymetallic Ore field, Guangxi. *Acta Geol. Sin.* **2008**, *82*, 967–977, (In Chinese with English Abstract).
56. Cheng, Y.S. Lead Isotope of Sulfide Minerals from Dachang Ore Field of Guangxi (South China): Characteristic and Implication. *Future Mater. Res. Ind. Appl.* **2012**, *455–456*, 1399–1403, (In Chinese with English Abstract). [[CrossRef](#)]